Antiferromagnetic coupling and impurity effects at junctions between Fe3O4 and Fe(001) layers

著者	Yanagihara H., Kamita H., Honda S., Inoue J., Kita Eiji, Itoh H., Mibu Ko

journal or publication title	Physical review B
volume	91
number	17
page range	174423
year	2015-05

URL	http://hdl.handle.net/2241/00125302

doi: 10.1103/PhysRevB.91.174423

Antiferromagnetic coupling and impurity effects at junctions between Fe_3O_4 and Fe(001) layers

H. Yanagihara,* H. Kamita, S. Honda, J. Inoue, and Eiji Kita
Institute of Applied Physics, University of Tsukuba, Tsukuba 305-8573, Japan

H. Itoh
Department of Pure and Applied Physics, Kansai University, Suita 564-8680, Japan

Ko Mibu
Graduate School of Engineering, Nagoya Institute of Technology, Nagoya 466-8555, Japan
(Received 27 May 2014; revised manuscript received 12 March 2015; published 20 May 2015)

We investigated the strong antiferromagnetic (AF) interlayer exchange coupling (IEC) at junctions between Fe(001) and Fe_3O_4(001) epitaxial films and the effects of an insertion layer of Mn or Co. In addition, we developed a nonlinear least-squares-fit technique to analyze the details of the magnetization processes and to distill the IEC constants. The analyses were performed by taking into account bilinear and biquadratic exchange couplings with a twisted magnetization state. The fitting results suggest the existence of significant distributions in bilinear and/or biquadratic IECs, which can originate from nonuniform stacking of atoms at the interface. The insertion of a Co layer with a thickness in the range of zero to two monolayers between the Fe_3O_4(001) and the Fe(001) layers significantly affects the magnetic-hysteresis (M-H) processes, whereas the insertion of a Mn layer does not. A quantitative fitting analysis of M-H curves suggests that the inserted thin Mn layer does not affect the AF-IEC significantly, whereas the Co layer suppresses the AF coupling and in fact is preferable for achieving ferromagnetic coupling, which is consistent with the tendency predicted by our theoretical model regarding impurity effects for the IEC of Fe/Fe_3O_4(001).

DOI: 10.1103/PhysRevB.91.174423 PACS number(s): 75.70.Cn, 73.20.−r, 71.55.−i

I. INTRODUCTION

The study of the interfaces of dissimilar classes of materials, such as metal/oxide [1,2] and organic/inorganic [3] interfaces has attracted considerable attention in light of interesting phenomena observed in such interfacial systems. The availability of the state-of-the-art technology of thin-film preparation combined with new theoretical insights has led to the discovery of various fascinating phenomena, such as two-dimensional high-mobility carriers [4] and interlayer exchange coupling (IEC) [5–8], including exchange bias [9]. Among the various oxide films, the perovskite family has been known to exhibit remarkable interfacial phenomena, whereas studies on spinel ferrite films and devices based on such films are relatively fewer than those on the perovskite films, probably due to the difficulties in controlling the spinel ferrite film quality, the complexity of the crystal structure, etc.

The phenomenon of IEC has been widely observed in various trilayer systems composed of two ferromagnetic metal/oxide films separated by a thin nonmagnetic film that is either a metal or an insulator [2,6,10–12]. The physics underlying IEC has been actively investigated because of its importance in terms of the development of both fundamental condensed-matter physics and magnetic device applications, such as spintronics for achieving antiparallel alignment of two ferromagnetic layers to suppress magnetostatic energy [13,14].

We have recently discovered that a bilayer system of Fe_3O_4/Fe(001) exhibits comparably strong antiferromagnetic (AF)-IEC at the interface [8,15]. The IEC energy in Fe_3O_4/Fe(001) was estimated as -2 erg/cm^2 from the magnetic-hysteresis (M-H) curves, and the IEC is isotropic [8,15]. The AF coupling constant is significantly large as a bilayer system of two ferromagnets. Here we reveal the details of the coupling mechanism and the interface structure at the two ferromagnetic layers.

The first-principles calculations for such systems result in a direct-type extremely large *ferromagnetic IEC* [16] that contradicts observations on assuming an ideally flat interface structure with wave functions strongly overlapped between the two ferromagnetic layers. This discrepancy suggests that either the interface state of the Fe_3O_4 layer is not simply metallic or a certain imperfection is present that weakens the coupling of the wave functions on both sides of the interface [16]. In fact, the junction of Fe_3O_4/Fe is highly resistive [17], which indicates that the overlap of the wave functions at the interface is weak.

Although it is not clear whether the mechanism of the IEC is intrinsic or extrinsic to such systems at the moment, it is known that the electronic state at the interface plays an important role in this exchange coupling. In this light, modifying the interface electronic state may provide the key to understanding this phenomenon. Recently, Inoue *et al.* suggested that the presence of an interface impurity state can cause extrinsic AF-IEC [18] of a reasonable magnitude under a certain condition. Our impurity theory also predicts that when Co is inserted between Fe and Fe_3O_4, the sign of the IEC becomes positive (ferromagnetic) whereas the insertion of Mn or Cr preserves or even enhances the AF-IEC.

In order to study the IEC in Fe_3O_4/Fe(001), including both bilinear and biquadratic components, we investigated the interface structure of Fe_3O_4/Fe(001) and developed nonlinear M-H curve-fit analyses. We also examined our impurity theory by inserting Mn or Co with various thicknesses between Fe

*yanagiha@bk.tsukuba.ac.jp

and Fe_3O_4. Our developed M-H curve-fit analysis yielded the quantitative values of both the bilinear and the biquadratic components for insertion layers of Mn or Co with various thicknesses.

In the following section, the experimental method will be explained. In Sec. III, the interface structure experimentally observed with transmission electron microscopy (TEM) and M-H curves of $Fe/X/Fe_3O_4(001)$ (X = Mn and Co) will be shown. A discussion of M-H curve analysis will be given in Sec. IV. A summary will be given in Sec. V.

II. EXPERIMENT

The study samples were grown by means of the O_2-assisted molecular-beam epitaxy (MBE) technique [8,15]. The typical base pressure was less than 1×10^{-8} Torr. All samples were grown on cleaved MgO(001) substrates with typical dimensions of $10 \times 20 \times 0.3$ mm^3. Before film growth, the substrates were annealed at 700 °C in a growth chamber to remove surface contaminants. After growing 20-nm-thick MgO(001) seed layers, Fe_3O_4 layers were grown by using a reactive MBE technique with oxygen gas at a substrate temperature of 270 °C. During Fe_3O_4 growth, the chamber pressure was maintained at 3×10^{-6} Torr. Fe layers were successively grown without oxygen flow at room temperature and under a pressure of approximately $\times 10^{-8}$ Torr. The film growth processes were monitored by reflection high-energy electron diffraction. In order to modulate the interface state, wedge-shaped thin doping layers of either Mn or Co with a thickness in the range of zero to two monolayers (MLs) were inserted by using a moving mask system.

The depth profiles of the inserted elements were confirmed by secondary ion mass spectroscopy, and the diffusion of Mn and Co was found to be negligible. The samples with the wedge-shaped doping layer were cut into six pieces along the direction perpendicular to the wedge slope. As shown in the insets of Figs. 2 and 3, we designed the samples with a region in which no Mn/Co insertion layer was deposited at one end of the films. The nominal thickness of the inserted layer for each piece is defined as the average thickness of the piece. $Fe_3O_4(001)$ films grown on MgO(001) exhibit a magnetization of 400 emu/cm^3, which value is slightly less than the magnetization of the bulk owing to the non-negligible amount of antiphase boundaries [19] located at the interface between MgO and Fe_3O_4. The sample structure is described as MgO(001)-substrate/MgO(20 nm)/Fe_3O_4(13 nm)/Mn or Co(zero to two ML)/Fe(9 nm)/Au(5 nm) in which the magnetic moments per unit surface area of the two ferromagnetic layers are approximately 0.52×10^{-3} emu/cm^2 for Fe_3O_4 and 1.53×10^{-3} emu/cm^2 for Fe.

III. EXPERIMENTAL RESULTS

A. Interface structure

Figure 1 shows a cross-sectional TEM image of the Fe_3O_4/Fe(001) bilayer system. The upper and lower halves of the image correspond to Fe and Fe_3O_4, respectively. From the image, we note the epitaxial growth of these two layers with the structure of MgO[100](001) ‖ Fe_3O_4[100](001) ‖ Fe[110](001). The lower half of the TEM image corresponding

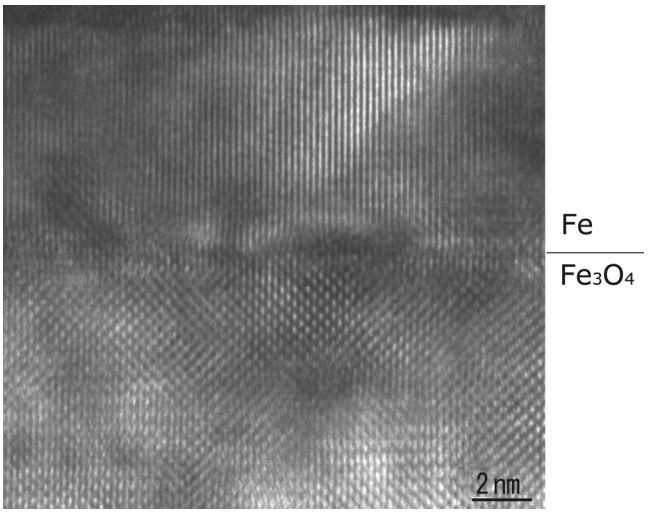

FIG. 1. Cross-sectional TEM image of the vicinity of the Fe_3O_4/Fe(001) interface.

to Fe_3O_4 is similar to that previously reported for Fe_3O_4 [19]. A few lattice displacements can be observed in the lattice image of the Fe_3O_4 region that may possibly be associated with antiphase-boundary-type defects [20,21]. It is evident that the interface structure is not atomically sharp. In certain structural sections, the columns of Fe atoms in the upper Fe layer are uniformly stacked on the Fe sites in the Fe_3O_4 layer; however, in other sections, the stacking is not uniform, irrespective of the arrangement of the columns of Fe in the Fe_3O_4 layer.

Because of the nonuniformity of the interface stacking, the IEC could originate from several different components depending on the local structures. We note that this type of growth is different from typical heteroepitaxial growth.

B. M-H curves of $Fe/X/Fe_3O_4(001)$ (X= Mn and Co)

The in-plane M-H curves for different insertion-layer thicknesses of Mn and Co at room temperature are shown in Figs. 2 and 3, respectively. In the case of the samples with Mn insertion layers, most of the samples with thicknesses in the range of $0 \leqslant t_{Mn} \leqslant 2.0$ ML exhibit magnetization processes with high saturation fields, which implies that the thin Mn layer does not suppress the AF-IEC. On the other hand, the AF-IEC in the samples with the Co insertion layers easily disappears for Co layers thicker than $\approx$1 ML, and it may change the sign from negative (antiferromagnetic) to positive (ferromagnetic). Upon comparing the tendencies of the M-H curves, we observed that the AF-IEC at the interface of Fe and $Fe_3O_4(001)$ is evidently affected by a thin insertion layer.

IV. M-H CURVE ANALYSIS

An experimentally obtained M-H curve at room temperature for the bilayer of 13-nm-thick Fe_3O_4 and 9-nm-thick Fe(001) is shown in Fig. 4. Least-squares-fit results of the four models are presented as well in the figure and will be discussed later. The saturation and residual magnetization correspond to the parallel and antiparallel alignments of the aforementioned thicknesses of the Fe_3O_4

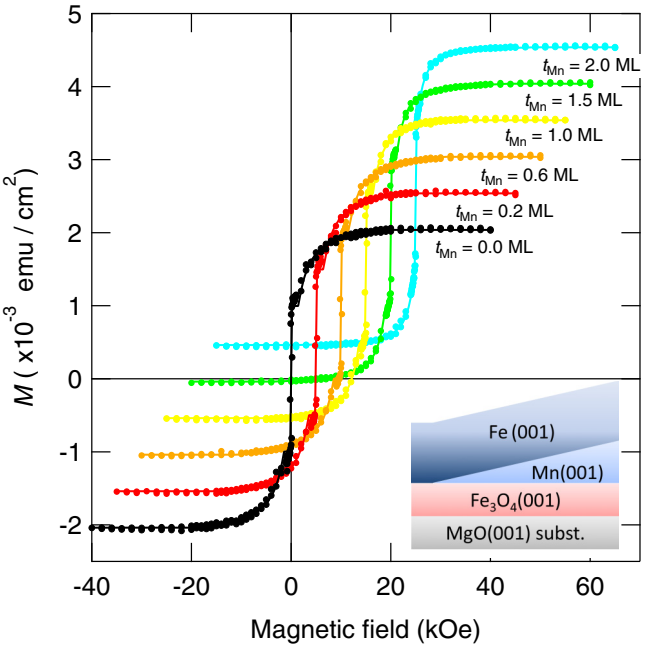

FIG. 2. (Color online) In-plane M-H curves for epitaxial films of Fe_3O_4/Mn(t_{Mn})/Fe(001) measured at room temperature. The origins of the M-H curves are shifted for clarity. The vertical axis corresponds to areal magnetization. The solid lines indicate the fitting results with the twist-J_1&J_2 model. The inset shows the schematic of the wedge-shaped stacking structure.

and Fe layers, respectively. Hereafter, we assume that the Fe_3O_4 and Fe films possess magnetizations of $M_{Fe_3O_4} = 400$

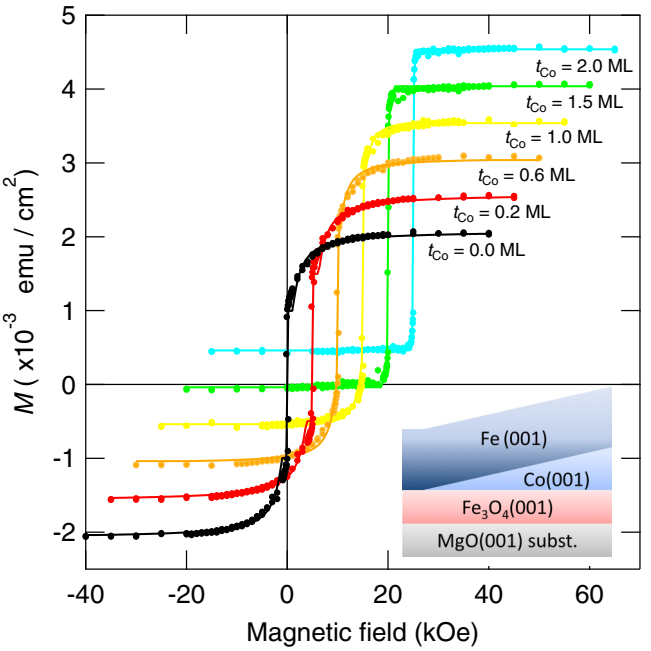

FIG. 3. (Color online) In-plane M-H curves for epitaxial films of Fe_3O_4/Co(t_{Co})/Fe(001) measured at room temperature. The origins of the M-H curves are shifted for clarity. The vertical axis corresponds to areal magnetization. The solid lines indicate the fitting results with the twist-J_1&J_2 model. The inset shows the schematic of the wedge-shaped stacking structure.

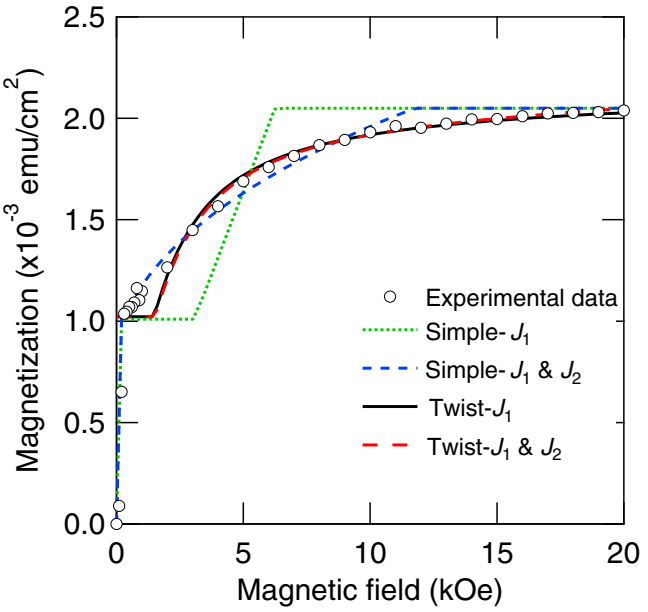

FIG. 4. (Color online) In-plane M-H curve for the bilayer of 13-nm-thick Fe_3O_4 and 9-nm-thick Fe(001) at room temperature. Open circles indicate experimental data. The fitting results of the simple-J_1, simple-J_1&J_2, twist-J_1, and twist-J_1&J_2 models and the experimental data are shown. Refer to the text for details of the corresponding models and the results of the fit.

and $M_{Fe} = 1700$ emu/cm^3, respectively. Because the M-H curves for inequivalent in-plane directions of $H \parallel [100]$ and $H \parallel [110]$ are almost the same and the M-H curve difference between the in-plane and the out-of-plane ones corresponds to the demagnetization energy for the Fe and Fe_3O_4 layers [8], we assume that the magnetic anisotropy term is negligible. The magnetization process is obviously nonlinear, meaning that the model of the two macrospins coupled to each other with a simple bilinear coupling (simple-J_1 model) shown by the dotted curve in Fig. 4 is not sufficient to explain the observed M-H process and that some modification of the model is required to reproduce the M-H process and to understand the IEC. We note that the IECs reported in Ref. [18] correspond to the estimation obtained by using the simple-J_1 model.

A. Model

There are several methods of extending the foregoing simple-J_1 model. The next simplest method is to add the higher-order terms of the IEC to the bilinear J_1; the biquadratic term J_2 is commonly utilized (simple-J_1&J_2 model) [22,23].

This model also treats each ferromagnetic layer as a single macrospin. A further extension is to consider the effect of the twisted magnetization state within each ferromagnetic layer along the normal to the film (twist-J_1 model) instead of the two solid macrospins. In this model, the interior spins have an additional degree of freedom such that the magnetization in each ferromagnetic layer is twisted due to a finite spin stiffness and Zeeman energy as shown in Fig. 5.

The third extension is to add the J_2 component to the twist-J_1 model (twist-J_1&J_2 model).

Unlike in the case of the simple-J_1 model, none of the M-H curves of the J_1&J_2, twist-J_1, or twist-J_1&J_2 models

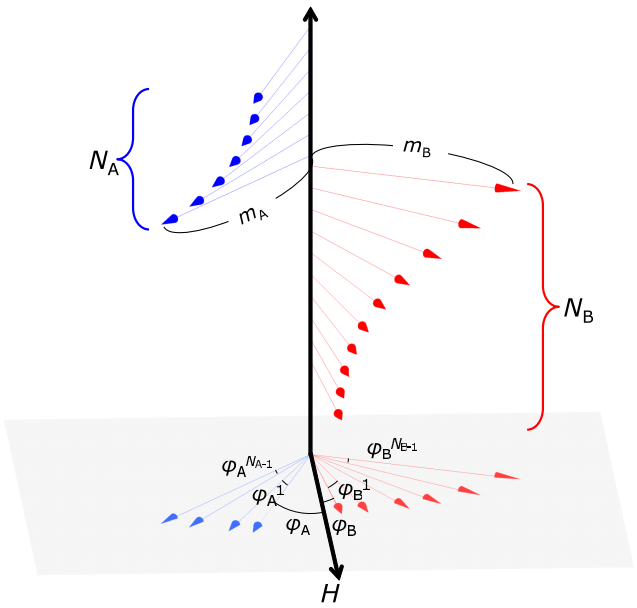

FIG. 5. (Color online) Twisted spin structure of antiferromagnetically coupled ferromagnetic layers.

can be solved analytically. Therefore, we perform a nonlinear least-squares fitting with every nonlinear objective function for the M-H curve to extract the coupling constant(s) from the experimentally obtained M-H data. The nonlinear M-H curve as an objective function is determined by the parameters of H, the layer magnetizations (M_A and M_B), the layer thicknesses (t_A and t_B), and the IEC (J_i), wherein A and B denote Fe_3O_4 and Fe, respectively.

The total free energy per unit area of the magnetically coupled bilayer system (F) is expressed as

$$F = E_Z + E_{ex}. \tag{1}$$

Here, E_Z and E_{ex} correspond to the Zeeman energy and exchange-coupling energy, respectively.

In the case of the simple-J_1&J_2 model, E_Z and E_{ex} can be written as follows:

$$E_Z = -HM_At_A\cos\theta_A - HM_Bt_B\cos\theta_B, \tag{2}$$

$$E_{ex} = -J_1\cos(\theta_A-\theta_B) - J_2\cos^2(\theta_A-\theta_B). \tag{3}$$

Here, $\theta_{A(B)}$ stands for the angle between the magnetization of the A(B) layer and the direction of the external field H.

On the other hand, the interior-twisted state with bilinear (and biquadratic) coupling at the interface (twist-J_1 model and twist-J_1&J_2 model) can be treated by modifying Motokawa's model [24] for a multilayer system [24,25]. E_Z and E_{ex} for a bilayer system, respectively, are described as

$$E_Z = -H\left[m_A\left\{\cos\phi_A + \sum_{n=1}^{N_A-1}\cos\left(\phi_A+\sum_{i=1}^{n}\phi_A^i\right)\right\} + m_B\left\{\cos\phi_B + \sum_{n=1}^{N_B-1}\cos\left(\phi_B+\sum_{j=1}^{n}\phi_B^j\right)\right\}\right], \tag{4}$$

$$E_{ex} = -A_Am_A^2\sum_{i=1}^{N_A-1}\cos\phi_A^i - A_Bm_B^2\sum_{j=1}^{N_B-1}\cos\phi_B^j - J_1\cos\left(\phi_A+\sum_{i=1}^{N_A-1}\phi_A^i-\phi_B-\sum_{j=1}^{N_B-1}\phi_B^j\right). \tag{5}$$

Here, $N_{A(B)}$ and $A_{A(B)}$ denote the number of subdivided layers and the exchange-coupling constant of the ferromagnetic layer A(B), respectively. The parameter $\phi_{A(B)}$ is defined as the angle between the direction of the endmost sublayer (which is farthest from the interface) and the external field. The parameter $\phi^i_{A(B)}$ denotes the angle between adjacent sublayers $m^i_{A(B)}$ and $m^{i+1}_{A(B)}$ (see Fig. 5). For the twist-J_1&J_2 model, a biquadratic term of $-J_2\cos^2(\phi_A+\sum_{i=1}^{N_A-1}\phi_A^i-\phi_B-\sum_{j=1}^{N_B-1}\phi_B^j)$ is added to the exchange-coupling energy of Eq. (5). The magnetization equilibrium conditions of the free energy result in the following recursive conditions:

$$\sin\phi^1_{A(B)} = \frac{H}{A_{A(B)}m_{A(B)}}\sin\phi_{A(B)},$$

$$\sin\phi^n_{A(B)} = \sin\phi^{n-1}_{A(B)} + \frac{H}{A_{A(B)}m_{A(B)}}\times\sin\left(\phi_{A(B)}+\sum_{i=1}^{n-1}\phi^i_{A(B)}\right). \tag{6}$$

Therefore, even in the twisted spin models, the pair of angles ϕ_A and ϕ_B determines the free energy of the system.

As shown above, once a series of the parameters of H, J_1,J_2, $A_{A,B}$, $m_{A,B}$, $N_{A,B}$,($M_{A,B}$), and ($t_{A,B}$) are given, the M-H curves can be numerically calculated by determining the two optimized parameters of $\phi_A(\theta_A)$ and $\phi_B(\theta_B)$ in the free-energy space for the twist-J_1 model and the twist-J_1&J_2 model (the simple-J_1&J_2 model). For determining the minimum value of F in the given parameter space, we used the downhill simplex method [26]. From the higher H for which all the moments definitely orient parallel to the external field, the optimized magnetization of each layer that minimizes F was determined sequentially with decreasing H. Using the obtained M-H curve for the given parameters as a trial function, the experimentally obtained data were fitted using a commercial least-squares-fit routine. We note that since the bilayer system treated here is fully epitaxial, the reasonable unit of twisted spins within each ferromagnetic layer is the lattice-plane spacing $d_{Fe} = 1.44\times10^{-8}$ and $d_{Fe_3O_4} = 2.10\times10^{-8}$ cm. For the Fe and Fe_3O_4 layers, we adopted the parameters $A_{Fe} = 4.4\times10^{11}$, $A_{Fe_3O_4} = 7.1\times10^{11}$ erg/cm^2, $m_{Fe} = 2.44\times10^{-5}$ emu/cm^2 (per sublayer), $m_{Fe_3O_4} = 8.40\times10^{-6}$ emu/cm^2 (per sublayer), $N_{Fe} = 62$, and $N_{Fe_3O_4} = 61$ from the bulk values.

B. Results of analysis and discussion

The nonlinear least-squares-fit results of the aforementioned four models (the simple-J_1, the J_1&J_2, the twist-J_1, and the twist-J_1&J_2) are shown in Fig. 4. The obtained fitting parameters for the four models are shown in Table I.

It can be observed that the fitting result of the simple-J_1 model is obviously poorer than those of the other three

TABLE I. Fitting results for the four models shown in Fig. 4.

	J_1 (erg/cm^2)	J_2 (erg/cm^2)
Simple-J_1	-2.42 ± 0.12	
Simple-J_1&J_2	-2.36 ± 0.20	-1.09 ± 0.12
Twist-J_1	-2.82 ± 0.63	
Twist-J_1&J_2	-2.76 ± 0.14	0.14 ± 0.45

models. The fitting results of J_1's for all four models are in good agreement with each other. On the other hand, J_2 seems dependent on the model. J_2 of the simple-J_1&J_2 model has the same order of magnitude as J_1. The simple-J_1&J_2 model nicely reproduces the M-H curve in the low-field region but cannot reproduce a smoothly saturating curve in the higher-field region. On the other hand, smoothly saturated M-H curves are reproduced without any kinks by the twisted spin models. Although there is no plateau at around the remanent state in the experimental data, a small but clear plateau appears in the M-H curve of both twisted spin models. We now discuss the possible reason why neither fit models of the simple-J_1&J_2 nor the twisted spin models can reproduce the overall observed M-H curve. In the real bilayer of the Fe/Fe_3O_4(001) system, there are various imperfections, such as the incoherent stacking at the interface as seen in Fig. 1, thickness fluctuations, and so on. Therefore the discrepancies in the M-H curves between the experiment and the fit models could be attributed to the existence of a distribution of the exchange couplings and/or the film thicknesses as the result of which it is hard to select the appropriate model from the standpoint of fitting results.

Upon comparing the simple-J_1&J_2 model and the twisted spin models, the latter models are more or less realistic because they take into account the internal degree of freedom of the ferromagnetic layers. Because both the 9-nm-thick Fe layer and the 13-nm-thick Fe_3O_4 layer are only an order of magnitude smaller than magnetic domain widths (w) both for Fe_3O_4 ($w = 72.8$ nm) [27] and Fe ($w = 64$ nm) [27] and the coupling constant J_1 at the interface is sufficiently large as shown in Table I, it is natural to consider that the twisted spin state is realized during the magnetization process.

Figure 6 shows the twisted spin variation at different external fields of the twist-J_1 model. For the time being, the J_2 term is omitted for simplicity. As can be seen in Fig. 6, the twisted spin state appears during the entire magnetization process except for the remanent state ($H = 0$) and the saturated state ($H \gtrsim 16$ kOe). The IEC constant inside the Fe layer is $m_{Fe}^2 A_{Fe} = 2.5 \times 10^2$ erg/cm^2 and that inside the Fe_3O_4 layer is $m_{Fe_3O_4}^2 A_{Fe_3O_4} = 5.0 \times 10^1$ erg/cm^2, respectively. In addition, $m_{Fe_3O_4}$ is smaller than m_{Fe}. Therefore the inside of the Fe_3O_4 layer is more twisted than that of the Fe layer. Although the value of J_1 is 1 to 2 orders smaller than $m_{Fe}^2 A_{Fe}$ or $m_{Fe_3O_4}^2 A_{Fe_3O_4}$, the twisted state is apparent in both sides of the interface with a thickness of $\sim$10 nm, especially under a high field. As shown earlier, the twisted spin state is significant in the M-H curves of our samples. It is hence more appropriate to analyze M-H data by taking the twisted spin into account.

In order to study the insertion-layer effect on the IEC, we performed nonlinear fitting (as mentioned earlier) of the twist-J_1&J_2 model. The insertion-layer-thickness dependences of

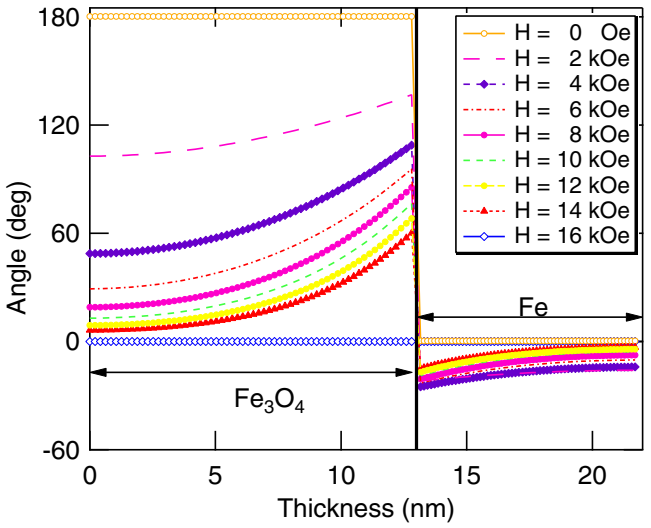

FIG. 6. (Color online) Variation in ϕ along the thickness of the bilayer at different fields as a fitting result for the twist-J_1 model. The corresponding M-H curve is shown as a black solid curve in Fig. 4. The spins of Fe and Fe_3O_4 are collinear only when $H = 0$ and $H \gtrsim 16$ kOe.

the fitting results of J_1 and J_2 are shown in Fig. 7. As qualitatively expected from Figs. 2 and 3, the fitting results of the J_1 values show a significant difference between the Mn- and the Co-based systems.

The effect of Mn-layer insertion on J_1 is relatively weak. On the other hand, the insertion effect of the Co layer appears significant. A Co thickness of less than one ML

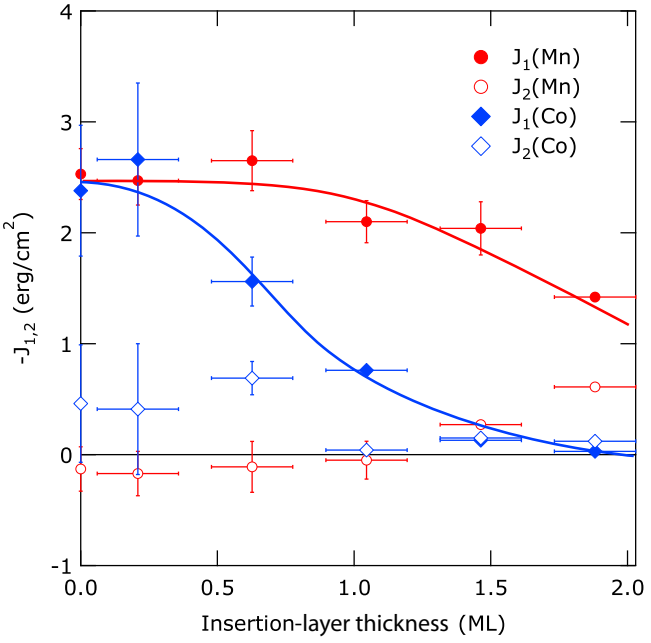

FIG. 7. (Color online) Insertion-layer-thickness dependence of J_1 and J_2 obtained by fitting of the twist-J_1&J_2 model. The vertical error bars are estimated by the least-squares fit of the M-H curves, and the horizontal ones are calculated considering the thickness variation in the insertion layers due to the wedged-slope structure. The solid lines serve as a visual guide.

destroys the strong J_1 observed in Fe/Fe_3O_4. According to the theoretical model of the IEC in $Fe/Fe_3O_4(001)$ [18], variation in the sign and magnitude of J caused by adding impurities at the interfaces is dependent on whether the impurity is Co or Mn owing to the change in the electronic states. The observed behavior of the impurity dependence of the sign of J is consistent with the conclusion drawn from the theoretical model, which means that this type of IEC is varied as the Slater-Pauling-like behavior. One can see that there is a slight discrepancy between the two M-H curves at around the remanent state for $Fe/Fe_3O_4(001)$ of Figs. 2 and 3 ($t_{Co,Mn} = 0$ ML). This may suggest that the interface structure is sensitive to the sample preparation.

In order to quantitatively evaluate the coupling constant and to establish a more comprehensive IEC model for this bilayer system, the details of the interface structure must be experimentally identified, which is an investigative challenge because the buried interface is composed of a complex surface of $Fe_3O_4(001)$. Since this system is composed of Fe, the interface environment can be probed through Mössbauer spectroscopy by inserting ^{57}Fe at the interface [28].

V. SUMMARY

To summarize, in order to examine the impurity effect on the IEC in a strongly coupled Fe_3O_4/Fe bilayer system, we prepared two films with wedge-shaped Co and Mn insertion layers with thicknesses ranging from zero to two MLs between Fe_3O_4 and Fe(001). We found that the observed nonlinear magnetization processes can be approximately reproduced by using the twisted magnetization model considering the bilinear IEC.

The slight discrepancy between the experimentally obtained M-H curves and the fitting results suggests that distribution of J and/or the thicknesses of the ferromagnetic layers are not negligible. For the case of the $Fe_3O_4/Co/Fe$ system, one ML of Co easily suppressed AF-IEC, whereas the AF-IEC of $Fe_3O_4/Mn/Fe$ showed less dependence on Mn-layer thickness. Applying our curve-fitting routine to M-H curves corresponding to different thicknesses of Co and Mn layers, we obtained the J_1 dependence of the impurity thickness. The effect of the impurity on J_1 is consistent with that predicted by the theory underlying the weakly coupled model. Our results indicate that the interface AF-IEC in Fe_3O_4/Fe can be controlled/tuned by inserting a very thin Co layer.

ACKNOWLEDGMENTS

H.Y. thanks S. Mitani for his guidance regarding previous studies on the twisted spin model. Magnetization measurements were performed at the Cryogenic Divisions of the Research Facility Center, University of Tsukuba. This work was supported by the Elements Science and Technology Project of Ministry of Education, Culture, Sports, Science, and Technology, Japan.

[1] J. J. Yang, M. D. Pickett, X. Li, D. A. A. Ohlberg, D. R. Stewart, and R. S. Williams, Nat. Nanotechnol. **3**, 429 (2008).
[2] A. Orozco, S. B. Ogale, Y. H. Li, P. Fournier, E. Li, H. Asano, V. Smolyaninova, R. L. Greene, R. P. Sharma, R. Ramesh, and T. Venkatesan, Phys. Rev. Lett. **83**, 1680 (1999).
[3] H. Ishii, K. Sugiyama, E. Ito, and K. Seki, Adv. Mater. **11**, 605 (1999).
[4] H. Y. Hwang, Y. Iwasa, M. Kawasaki, B. Keimer, N. Nagaosa, and Y. Tokura, Nat. Mater. **11**, 103 (2012).
[5] J. Faure-Vincent, C. Tiusan, C. Bellouard, E. Popova, M. Hehn, F. Montaigne, and A. Schuhl, Phys. Rev. Lett. **89**, 107206 (2002).
[6] R. E. Camley and D. R. Tilley, Phys. Rev. B **37**, 3413 (1988).
[7] H.-C. Wu, S. K. Arora, O. N. Mryasov, and I. V. Shvets, Appl. Phys. Lett. **92**, 182502 (2008).
[8] H. Yanagihara, Y. Toyoda, A. Ohnishi, and E. Kita, Appl. Phys. Express **1**, 111303 (2008).
[9] J. Nogués and I. K. Schuller, J. Magn. Magn. Mater. **192**, 203 (1999).
[10] S. S. P. Parkin, Phys. Rev. Lett. **67**, 3598 (1991).
[11] T. Katayama, S. Yuasa, J. Velev, M. Y. Zhuravlev, S. S. Jaswal, and E. Y. Tsymbal, Appl. Phys. Lett. **89**, 112503 (2006).
[12] H. Yanagihara, Y. Toyoda, and E. Kita, J. Appl. Phys. **101**, 09D101 (2007).
[13] *Ultrathin Magnetic Structures I*, edited by J. A. C. Bland and B. Heinrich (Springer-Verlag, Berlin/Heidelberg, 1994).
[14] *Ultrathin Magnetic Structures IV*, edited by J. A. C. Bland and B. Heinrich (Springer, Berlin, 2005).
[15] H. Yanagihara, Y. Toyoda, and E. Kita, J. Phys. D: Appl. Phys. **44**, 64011 (2011).
[16] T. Kida, S. Honda, H. Itoh, J. Inoue, H. Yanagihara, E. Kita, and K. Mibu, Phys. Rev. B **84**, 104407 (2011).
[17] H. Yanagihara, K. Shimada, T. Niizeki, E. Kita, J. Inoue, A. Fukushima, and S. Yuasa, J. Appl. Phys. **113**, 17B104 (2013).
[18] J. Inoue, S. Honda, H. Itoh, K. Mibu, H. Yanagihara, and E. Kita, Phys. Rev. B **85**, 184431 (2012).
[19] D. T. Margulies, F. T. Parker, F. E. Spada, R. S. Goldman, J. Li, R. Sinclair, and A. E. Berkowitz, Phys. Rev. B **53**, 9175 (1996).
[20] D. T. Margulies, F. T. Parker, M. L. Rudee, F. E. Spada, J. N. Chapman, P. R. Aitchison, and A. E. Berkowitz, Phys. Rev. Lett. **79**, 5162 (1997).
[21] W. Eerenstein, T. T. M. Palstra, T. Hibma, and S. Celotto, Phys. Rev. B **68**, 014428 (2003).
[22] M. Röhrig, R. Schäfer, A. Hubert, R. Mosler, J. A. Wolf, S. Demokritov, and P. Grünberg, Phys. Status Solidi A **125**, 635 (1991).
[23] E. E. Fullerton, K. T. Riggs, C. H. Sowers, S. D. Bader, and A. Berger, Phys. Rev. Lett. **75**, 330 (1995).
[24] M. Motokawa, Prog. Theor. Phys. Suppl. **101**, 537 (1990).
[25] M. Motokawa and H. Dohnomae, J. Phys. Soc. Jpn. **60**, 1355 (1991).
[26] W. H. Press, S. A. Teukolsky, W. T. Vetterling, and B. P. Flannery, *Numerical Recipes in C*, 2nd ed. (Cambridge University Press, Cambridge, UK, 1992) .
[27] J. M. D. Coey, *Magnetism and Magnetic Materials* (Cambridge University Press, New York, 2009), p. 625.
[28] K. Mibu, M. Seto, T. Mitsui, Y. Yoda, R. Masuda, S. Kitao, Y. Kobayashi, E. Suharyadi, M. Tanaka, M. Tsunoda, H. Yanagihara, and E. Kita, Hyperfine Interact. **217**, 127 (2012).